Available online at www.sciencedirect.com
ScienceDirect
Optics Communications 268 (2006) 253–260
OPTICS COMMUNICATIONS
www.elsevier.com/locate/optcom

Scanning two photon fluorescence microscopy with extended depth of field

E.J. Botcherby, R. Juškaitis, T. Wilson *

University of Oxford, Department of Engineering Science, Parks Road, OX1 3PJ, UK

Received 28 June 2006; accepted 14 July 2006

Abstract

We describe the design and implementation of a light efficient binary phase-only diffraction optical element which converts a laser beam into an annular ring with the loss of less than 25% of the overall power. The use of annular illumination permits us to obtain an increase in the axial extent of the point spread function of a microscope objective without compromising the lateral resolution. The light efficiency of the system permitted two photon fluorescence images with extended depth of field to be obtained. The combination of two such extended depth of field images obtained at different parallaxes allowed the generation of high resolution two photon stereo pairs.

Keywords: Two photon fluorescence microscopy; Extended depth of field; Diffractive optics

1. Introduction

One of the most important factors in determining the imaging properties of an optical microscope is the form of the focussed spot of light which probes the specimen. The ability to tune the form of this point spread function (PSF) by the careful control of the optical field incident on the objective lens pupil has lead to the field of point spread function engineering. Specific applications involve attempts at super-resolution [1–4], adaptive optics [5], the control of polarization of the focal spot [6–8], and the whole field of Meso-Optics (see e.g. [9]). A particularly simple and intriguing application is to produce an axially extended PSF without sacrificing lateral resolution. It has long been known that by illuminating the back aperture of an objective lens with a ring of light a PSF of considerable axial extension would result [10–12]. There are a number of ways to produce annular illumination. The simplest is to insert a physical annular mask into the pupil plane of the objective lens so as to permit only a ring of light to be transmitted. This is clearly undesirable since most of the incident energy is blocked leading to a very poor use of the available light. An alternative approach uses a conical lens or axicon [9,13]. Although this is a light efficient method to produce ring illumination it does, as we shall see later, have some drawbacks for microscopy applications. In the following, therefore, we shall discuss the design of a circularly symmetric binary phase-only grating and show that this may be used in a highly light efficient manner to produce ring illumination in a manner suitable for use in microscopy.

As an application we shall concentrate on scanning two photon fluorescence microscopy [14]. We choose this imaging mode since it possesses an inherent optical sectioning effect due to the non-linear fashion in which the fluorescence is generated. This in turn implies it is not possible to image a whole volume specimen without stitching together a whole through-focus series of images unless a point spread function of considerable axial extent is used. Further the non-linear nature of the excitation process requires that the available light be used in the most efficient way. We shall demonstrate that the light efficiency of our

* Corresponding author.
E-mail address: tony.wilson@eng.ox.ac.uk (T. Wilson).

0030-4018/$ - see front matter © 2006 Elsevier B.V. All rights reserved.
doi:10.1016/j.optcom.2006.07.026

binary phase grating is such that we can generate two-photon extended depth of focus images with ease. We note that this would not be practical if a physical annular stop was used to produce the ring illumination. Our system design is such that we lose less than 25% of the overall laser power and are able to tune the shape of the PSF to be essentially flat over more than a 10 μm range. A further advantage of our approach is that by carefully tuning the directions along which our extended depth of focus images are obtained it is possible to obtain high-resolution two-photon fluorescence stereo image pairs.

2. Theory-system design

A schematic of the system that we will use is shown in Fig. 1. A Gaussian laser beam ($E \propto \exp(-r^2/w^2)$, where r is the radial coordinate and w is the width of the beam), illuminates an optical element with amplitude transmission function $T(r)$ placed in the back focal plane of a lens with focal length f. The Fourier transform of the amplitude which is transmitted, $T(r)\exp(-r^2/w^2)$, appears in the Fourier plane of the lens. This field, $P(R)$, may be written, due to circular symmetry of our problem [15] as

$$P(R) = \int_0^\infty T(r)\exp(-r^2/w^2)J_0\left(\frac{2\pi rR}{\lambda f}\right)2\pi r\,\mathrm{d}r, \tag{1}$$

where R represents the radial coordinate in the Fourier plane of the lens, J_0 is the zeroth order Bessel function of the first kind and λ is the wavelength. We position an objective lens such that its pupil plane is coincident with the Fourier plane of the first lens so that $P(R)$, Eq. (1), becomes the effective pupil function of the objective lens. In the low numerical aperture case the field in the focal region of the objective lens is given by the Fourier transform of the pupil function $P(R)$ however the situation is slightly more complicated for high NA objectives because substantial portions of the wavefront are refracted through large angles and the vectorial nature of light becomes important. Formal expressions for the field produced by a high NA objective lens have already been evaluated [16]. For the case where the illumination is uniform and linearly polarized in the x-direction, the field is given by

$$\mathbf{E}(r,\phi,z) = \frac{\pi \mathrm{i}}{\lambda}\begin{pmatrix} I_0 + I_2\cos 2\phi \\ I_2 \sin 2\phi \\ -2\mathrm{i}I_1\cos\phi \end{pmatrix}, \tag{2}$$

where the integrals I_0, I_1 and I_2 are defined in our case as

$$I_0 = \int_0^\alpha P(\theta)\cos^{1/2}\theta\sin\theta(1+\cos\theta)J_0(kr\sin\theta)\mathrm{e}^{-\mathrm{i}kz\cos\theta}\,\mathrm{d}\theta, \tag{3}$$

$$I_1 = \int_0^\alpha P(\theta)\cos^{1/2}\theta\sin^2\theta J_1(kr\sin\theta)\mathrm{e}^{-\mathrm{i}kz\cos\theta}\,\mathrm{d}\theta, \tag{4}$$

$$I_2 = \int_0^\alpha P(\theta)\cos^{1/2}\theta\sin\theta(1-\cos\theta)J_2(kr\sin\theta)\mathrm{e}^{-\mathrm{i}kz\cos\theta}\,\mathrm{d}\theta. \tag{5}$$

J_1 and J_2 represent first and second order Bessel functions of the first kind respectively, ϕ is the azimuthal angle in the focal region and α is the maximum angle of convergence of the objective lens. $P(\theta)$ is the pupil function evaluated in Eq. (1) with the transformation $R = f_0\sin\theta$ where f_0 is the effective focal length of the objective lens.

We note that for the case where the pupil is apodized such that the pupil function may be described by an infinitely narrow annulus, $P(\theta) = \delta(\theta - \alpha)$, the field becomes a Bessel beam and the focal intensity is given by:

$$\begin{aligned}|E|^2 \propto{}& [1+\cos\alpha]^2 J_0^2(kr\sin\alpha) + [1-\cos\alpha]^2 J_2^2(kr\sin\alpha) \\ &+ [2\sin^2\alpha J_0(kr\sin\alpha)J_2(kr\sin\alpha)\cos 2\phi] \\ &+ 4J_1^2(kr\sin\alpha)\cos^2\phi,\end{aligned} \tag{6}$$

which does not vary with axial position z. Indeed in the low aperture limit we note that this expression results in the familiar $|E|^2 \propto J_0^2(kr\sin\alpha)$ Bessel beam. Although this situation cannot be realized practically, this example demonstrates that PSF elongation can be achieved as a direct result of annular illumination. We will now explore various methods for producing annular illumination in a light efficient manner. It will be shown that by far the most satisfactory of these methods is to use a binary phase grating. We began by considering an axicon which is a conical lens which introduces a phase variation that is a linear function of radial position. There are two varieties of axicon whose profiles are shown in Fig. 2, namely positive and negative ones. These elements can be described by the following transmission functions:

$$T_{\mathrm{pos}}(r) = \mathrm{e}^{\mathrm{i}2\pi tr}, \tag{7}$$

$$T_{\mathrm{neg}}(r) = \mathrm{e}^{-\mathrm{i}2\pi tr}, \tag{8}$$

where t is the parameter describing the slope of the axicon.

If we use such axicons as the optical elements in the system of Fig. 1 then the effective pupil function $P(R)$ is annular in form and the resulting intensity along the optical axis ($r = 0$) in the focal region of the objective is given by

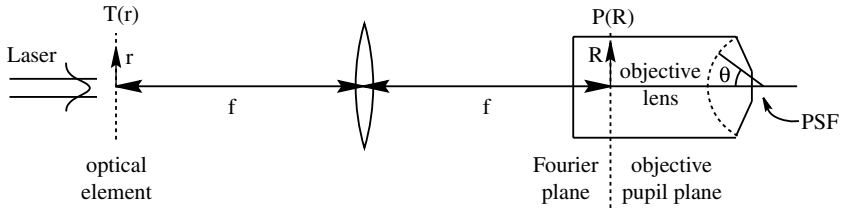

Fig. 1. Schematic diagram of the optical system.

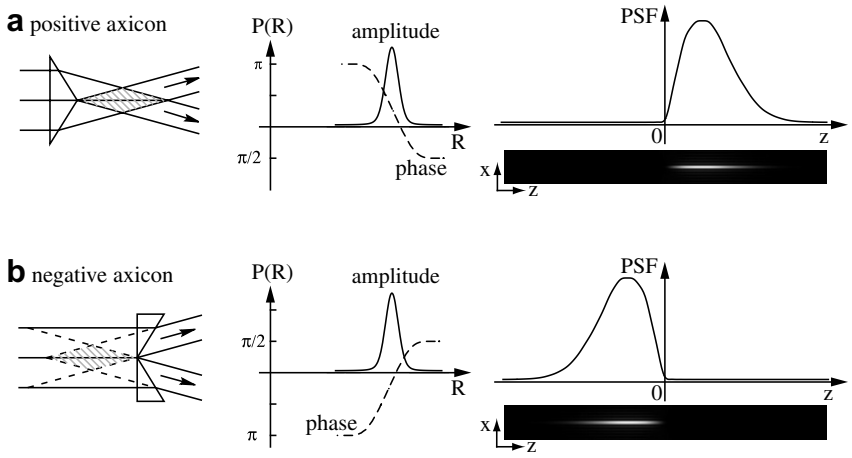

Fig. 2. The pupil function and corresponding intensity profile of the PSF generated by (a) a positive axicon and (b) a negative axicon. Parameters – $w = 0.5$ mm, $t = 25$ mm^{-1}, $\lambda = 750$ nm, $f = 106.66$ mm, $NA = 1.4$ oil immersion.

$|E|^2 \propto |I_0|^2$. These results are shown graphically in Fig. 2. We note that both the positive and negative axicons produce essentially ring illumination which gives rise to the desired axial elongation. However since the effective pupil functions are complex – the phase varies roughly linearly over the region where the intensity is significant – the distribution is asymmetric about the focal plane.

The asymmetry, with respect to the focal plane ($z = 0$), of both these PSFs suggests that we might be able to produce an even larger axial extension if we use an optical element possessing a phase variation equivalent to the superposition of both a positive and a negative axicon. However, since the pupil function phase produced by each individual axicon is equal and opposite in magnitude, it is important to be able to control the relative phase between these elements so that their PSFs combine constructively in the focal plane of the objective lens. One method by which the transmission functions of Eqs. (7) and (8) can be combined and the relative phase between their contributions controlled is to use a binary, phase only, mask whose transmission function is shown in Fig. 3. Mathematically this can be expressed using a Fourier series

$$T(r) = \frac{4}{\pi}\sum_{N=0}^{\infty}\frac{(-1)^N}{2N+1}\cos[(2N+1)(2\pi tr-\beta)] = \frac{4}{\pi}\left\{\cos[2\pi tr-\beta]-\frac{1}{3}\cos[3(2\pi tr-\beta)]+\frac{1}{5}\cos[5(2\pi tr-\beta)]\ldots\right\} \quad (9)$$

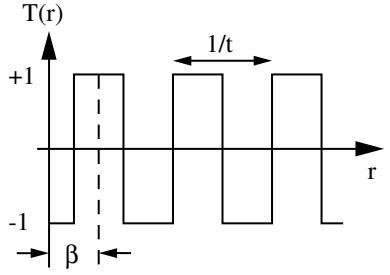

Fig. 3. The phase grating transmission function given in Eq. (9).

where β is an arbitrary phase offset. The important point to notice is that the average of this function $T(r)$ is zero and hence there is no zero spatial frequency term in the Fourier expansion. Physically this means that no light is directed to the zeroth diffraction order and it is this which accounts for the high throughput efficiency of our approach.

It is apparent that by setting $\beta = 0$ the first term in Eq. (9) becomes $\cos[2\pi tr] = \frac{1}{2}[e^{i2\pi tr} + e^{-i2\pi tr}]$ which is equivalent to the superposition of a positive and negative axicon. This leads to an annular ring whose amplitude is purely real and hence the resulting PSF, which is the superposition of the individual axicon PSFs, becomes symmetric about the focal plane. Higher diffraction orders do not contribute due to the limited aperture of the objective lens. Fortunately these contain far less energy than the first order as they are represented by less dominant terms in the series. The overall throughput efficiency of light into the first order is calculated numerically to be 81.0%.

The effect of choosing a non-zero value of β superposes the two axicons with relative phase shift 2β. This is illustrated in Fig. 4 for the cases where $\beta = 0$ and $\beta = \pi/4$. In both cases we observe an undesired dip in PSF intensity at the focal plane. The origin of this dip may be understood from the detailed form of the annular illumination presented to the pupil of the objective lens. This effective pupil function is shown in Fig. 4 where it is seen that over a significant region the pupil function is negative. The effect of choosing $\beta = \pi/4$, for instance, is to produce the desired sharp ring illumination together with two, (undesired) negative lobes on each side. These negative lobes are in fact the cause of the undesired dip in intensity in the focal plane and may be removed by introduction of an apodization mask. Fig. 5 shows the pupil plane field for the case of $\beta = \pi/4$ and the effect of inserting an apodization mask of width $2d$ on the axial intensity profile as a function of d.

This was calculated numerically by inserting the phase grating transmission function of Eq. (9) into Eqs. (1)–(5). To account for the effect of the apodization mask, integrals Eqs. (3)–(5) where taken between angular limits

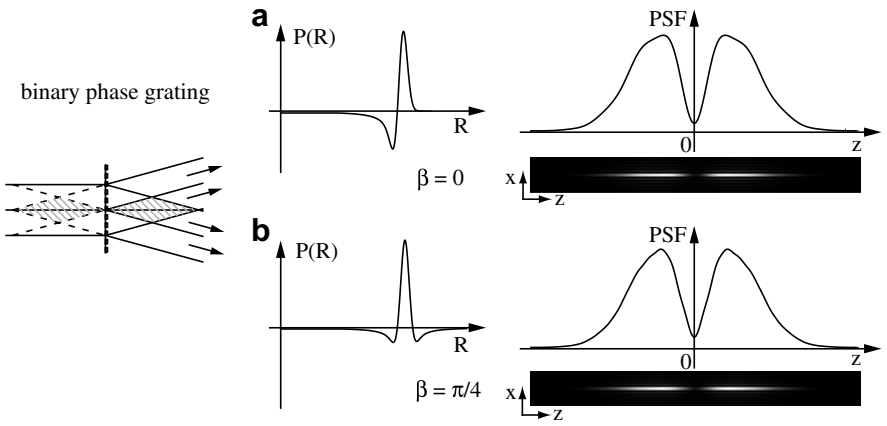

Fig. 4. The pupil function and corresponding intensity profile of the PSF generated by the binary phase grating defined in Eq. (9) with (a) $\beta = 0$ and (b) $\beta = \pi/4$. (Note that the phase variations from each axicon cancel out in the pupil plane to produce a pupil function that is entirely real.)

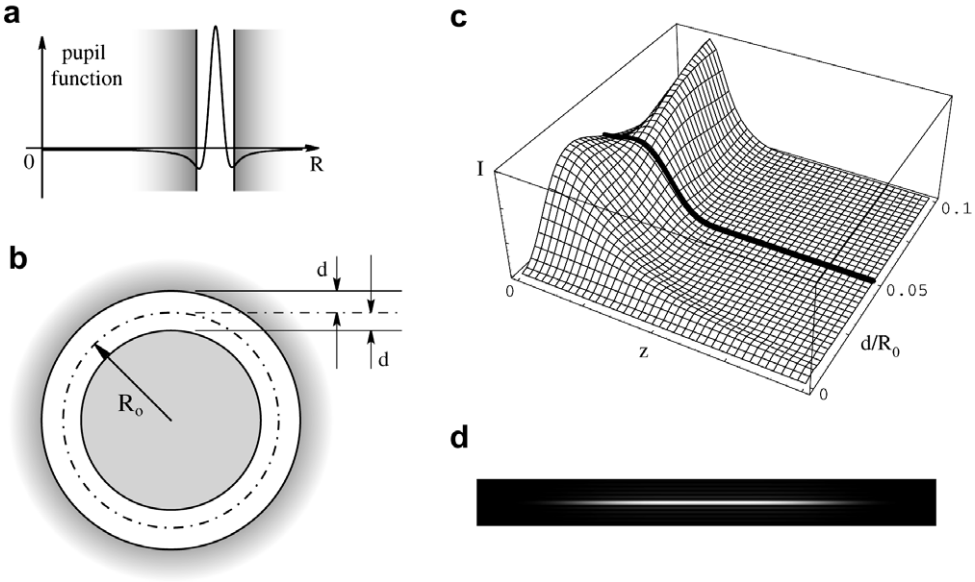

Fig. 5. (a) An illustration of how the apodization mask truncates the field in the pupil plane when $\beta = \pi/4$. (b) A further 2D illustration of the same apodization mask and definition of the parameters d and R_0. (c) The axial intensity profile of the PSF generated as a function of d/R_0 with the optimally flat PSF marked, (d) the XZ intensity profile of the PSF for this optimal case. (N.B. $R_0 = t\lambda f$ gives the approximate position of the peak of the ring.)

corresponding to the edges of the mask. From this plot we can see that reducing the value of d reduces the central dip in the distribution at the cost of overall PSF length. The specific case where the ripple is reduced to zero ($d^2I/dz^2(0) = 0$) is highlighted on the graph. A further plot of the PSF in the xz plane is shown in Fig. 5d for this optimum case. In practice a larger value than the optimum was selected for d as it was considered to be of more practical interest to extend the PSF than to reduce the ripple completely.

Finally we mention the fact that apodizing the pupil function unavoidably blocks some of the incident light energy and therefore reduces throughput efficiency. A new calculation however reveals that 77.3% still enters the final PSF from the incident laser beam. This high efficiency is extremely important when operating in the two photon fluorescence regime.

3. Experimental

Fig. 6 shows a schematic of the system used. In all experiments we employed a Ti:Sapphire laser (*Tsunami*, Spectra Physics) with a maximum available power of 630 mW, tuned to wavelength 750 nm. For two photon imaging, the laser was operated in a modelocked regime, which produced pulses of length ~100 fs at a repetition rate of 80 MHz. The power could be adjusted externally with a neutral density filter set. A telescope arrangement (not shown) was also used to adjust the beam width illuminating the phase grating. This was necessary in order to match the diffraction pattern produced by the grating to the (fixed) width of the apodization mask.

The binary phase plate was produced by a two step process. First a chromium-on-glass photolithographic mask consisting of a set of concentric rings having equal

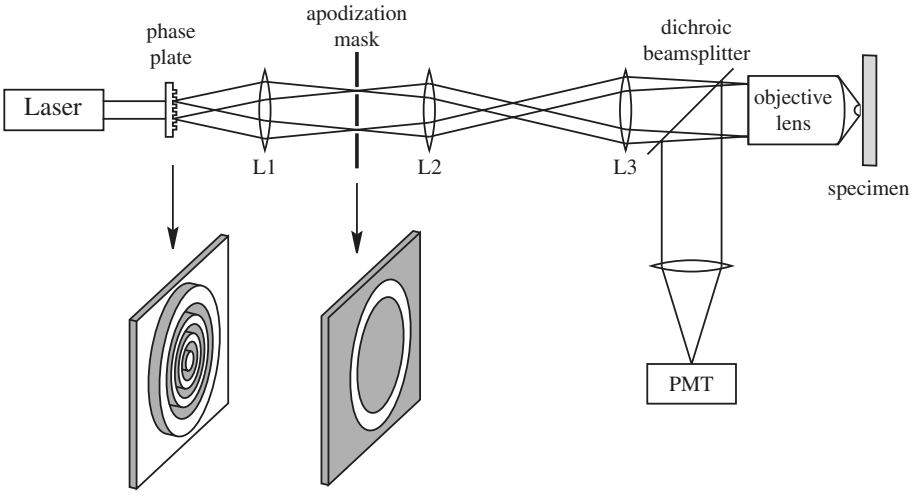

Fig. 6. Schematic diagram of the experimental arrangement. The phase plate is placed in the front focal plane of lens L1 and the apodization mask is located in the back focal plane. Lenses L2 and L3 constitute a 4*f* system which images the apodized annular illumination into the pupil plane of the objective.

mark-to-space ratio with spatial frequency of $t = 25\ \mathrm{mm}^{-1}$ was made using commercially available mask fabrication techniques (JD Phototools, Manchester, UK). This mask was then used to expose a glass substrate spin-coated with a layer of photoresist. After this the photoresist from unexposed areas was removed leaving a clear glass surface. The thickness of the film was chosen to ensure that light travelling through areas where the film had been deposited became exactly out of phase with light travelling through film-free areas for $\lambda = 750$ nm (equivalent to the transmission function in Fig. 3). The apodization mask was also made using the same technology but in this case the chromium-on-glass master was used directly.

The elements of the optical train were linked by achromatic doublet lenses. It is important to note that compared to Fig. 1 our experimental setup in Fig. 6 included an extra 4*f* imaging stage. This was for two reasons: first, the pupil plane of high NA objective lenses is positioned inside the lens body and hence it would be impossible to physically place the apodization mask in this position. Second, having an extra imaging stage allowed us certain flexibility in matching objective lenses with different pupil sizes to the fixed diameter of our annular ring.

The specimens were mounted on a high precision scanning stage (P-611.3S NanoCube, PI Instruments, Karlsruhe) which provided a scanning range of 100 μm in all three dimensions and could be easily reconfigured between X–Y and X–Z scans. Signal detection was provided by a large area photomultiplier, which was coupled to the objective lens via a dichroic beamsplitter.

In order to characterize the imaging properties of our system we began by measuring its illumination PSF. This can be done in a variety of ways but the most direct is to use of a sub-resolution scatterer. This method has the added advantage of producing data with a very good signal-to-noise ratio and hence is capable of revealing fine details in the shape and orientation of the PSF which helps with aligning the illumination optics.

We chose to use colloidal gold particles (British BioCell International) of nominal diameter 100 nm, which have been shown previously to be a good approximation to dipole scatterers [17]. The assumption of dipole scattering permits us to write an expression for the image formed in our system (essentially a conventional microscope) as [17]

$$I(r,\phi,z) = (|I_0|^2 + (I_0 I_2^* + I_0^* I_2)\cos 2\phi + |I_2|^2)(f_0 + f_2) + 16|I_1|^2 f_1 \cos^2\phi, \tag{10}$$

where I_0, I_1 and I_2, are once again given in Eqs. (3)–(5). This expression again assumes that the input illumination is linearly polarized in the pupil plane along the x-direction. The constants f_0, f_1 and f_2 are related to the detection efficiency for the scattered light assuming that light is collected over the the full extent of the objective aperture. Expressions for these are given by:

$$f_0 = \int_0^{\alpha} (1+\cos\theta)^2 \sin\theta \cos^{1/2}\theta \,\mathrm{d}\theta, \tag{11}$$

$$f_1 = \int_0^{\alpha} \sin^2\theta \cos^{1/2}\theta \,\mathrm{d}\theta, \tag{12}$$

$$f_2 = \int_0^{\alpha} (1-\cos\theta)^2 \sin\theta \cos^{1/2}\theta \,\mathrm{d}\theta, \tag{13}$$

where α is the maximum angle of convergence of the objective lens used. Fig. 7 shows numerical simulations of the images generated by scanning a gold bead in the XY and XZ planes using a 1.4 NA 63 X Zeiss oil immersion objective lens with the following (experimental) parameters – $w = 0.8$ mm, $t = 25\ \mathrm{mm}^{-1}$, $\lambda = 750$ nm, $R_0 = 3.33$ mm (as measured in the objective pupil plane), $d/R_0 = 0.05$.

The sample for this experiment was made by diluting a suspension of gold beads, drying a drop of this solution onto a coverslip and then mounting it with immersion oil

onto a microscope slide. The image of one such gold bead taken with our system is also shown in Fig. 7 and exhibits a pleasing match with the theoretical simulations shown on the same figure.

We then proceeded to measure the two-photon fluorescence PSF directly by using fluorescent polymer beads rather than gold beads. Since the overall PSF is the square of the illumination PSF we can see from Fig. 7, which is effectively the illumination PSF, that the relatively small dip in the middle of the figure will be further emphasized when squared. We were therefore compelled to chose a different set of illumination parameters corresponding to less aggressive depth extension in order to flatten the resulting PSF.

If we assume that the sub-resolution fluorescent object emits fluorescence radiation isotropically at a rate proportional to the square of the illumination intensity then we may write the image intensity as:

$$I(r,\phi,z) \propto \left\{ |I_0 + I_2 \cos 2\phi|^2 + |I_2 \sin 2\phi|^2 + |2I_1 \cos \phi|^2 \right\}^2, \tag{14}$$

where I_0, I_1 and I_2, are once again given by Eqs. (3)–(5). Using the set of parameters $w = 0.5$ mm, $t = 25\ \text{mm}^{-1}$, $\lambda = 750$ nm, $R_0 = 3.33$ mm, $d/R_0 = 0.05$, $NA = 1.4$ oil immersion we arrived at the numerical simulation shown in Fig. 8.

Our sample for this experiment was a fluorescent polymer beads (Molecular Probes Fluosphere 505/515 dia ≈ 200 nm). When imaging this sample a dichroic beam-splitter and band pass filter were used in the detection path to separate out the two photon fluorescence signal from miscellaneous reflections of the laser beam. An example image of one such polymer bead is shown in Fig. 8, again in correspondence with the theoretical plot.

It is worth noting that despite the fact that the bead size has increased by a factor of two (and thus the number of available fluorescent molecules by a factor of eight) as compared to the 100 nm beads we used before, the signal-to-noise ratio in Fig. 8 is still significantly worse than that in Fig. 7. This signal-to-noise was further compromised by the fact that the imaging of the beads was accompanied by severe photobleaching and hence no averaging was possible. This in our opinion makes the scatter method far more reliable and accurate for probing imaging properties of the two-photon microscope.

We now show examples of images taken using the extended depth of focus PSF generated with the binary phase grating and apodization mask. We chose as our test specimen a particular type of pollen grain from the Asteraceae family that is found in a commercial sample (Carolina w.m. 30-4264 (B690)). This specimen, with a diameter of ≈ 20 μm, was of particular interest to us because of its micro-spikes. These are useful for demonstrating the lateral resolution of our system.

For comparison purposes, we modified our system to enable us to acquire standard, non extended depth, two-photon fluorescence images. This was done by removing all the masks from the path and expanding the beam to fill the back aperture of the objective lens. An image of our test specimen taken with a single XY scan is shown in Fig. 9a and this clearly demonstrates the sectioning capability of two photon systems due to the restricted axial extent of the PSF.

Returning to the setup in Fig. 6 an image of a similar pollen grain was acquired with a single frame scan. This image, which is shown in Fig. 9b, clearly demonstrates the effect of our extended depth of focus PSF. In this case it is clear that information from a whole range of depths is presented simultaneously. Broadly speaking, this is equivalent to taking a number of scans with the normal two photon microscope and superimposing them on top of each other. In this respect it could be regarded as a two-photon counterpart of a well known extended focus imaging modality in confocal fluorescence microscopy [18]. Furthermore it can be seen that the lateral resolution has in no way been compromised in this image.

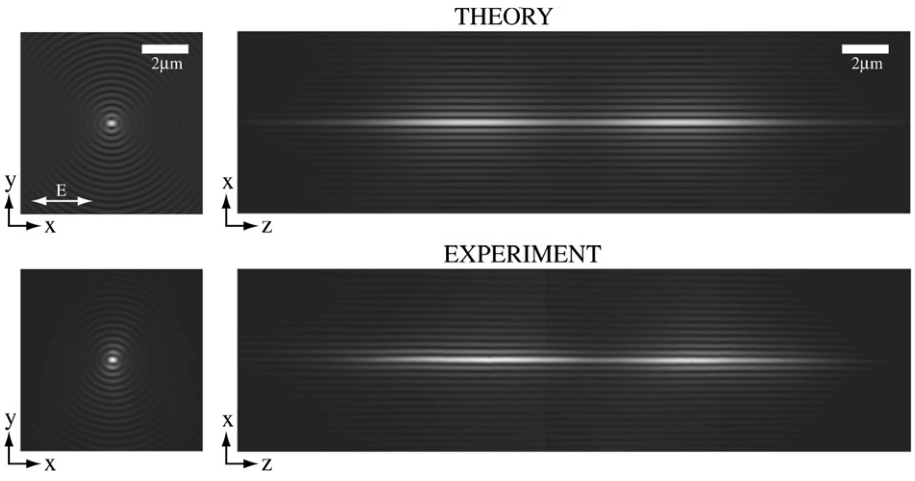

Fig. 7. Numerical simulations (top) and the corresponding experimental images (bottom) generated by scanning a sub-resolution gold bead in the XY and XZ planes in reflection mode using annular illumination. See text for parameters used.

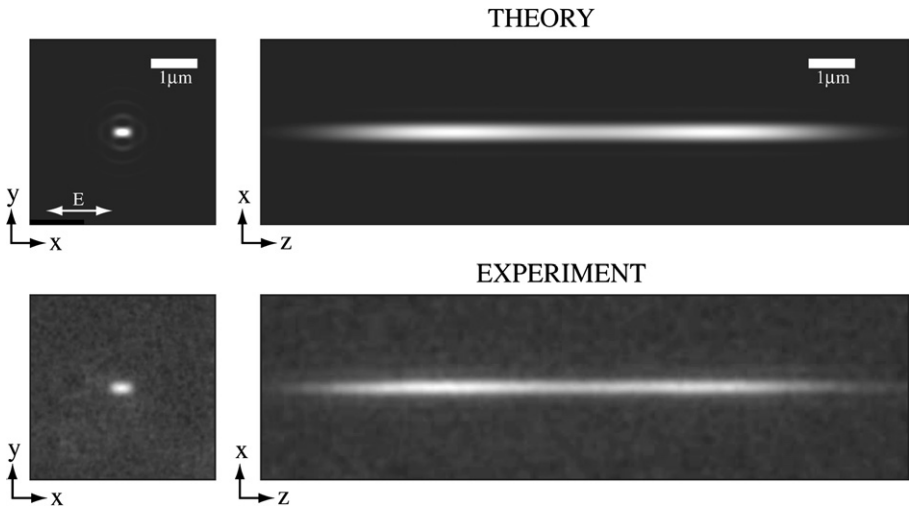

Fig. 8. Numerical simulations (top) and the corresponding experimental images (bottom) generated by scanning a sub-resolution fluorescent polymer bead in the XY and XZ planes in two-photon fluorescence mode using annular illumination. See text for parameters used.

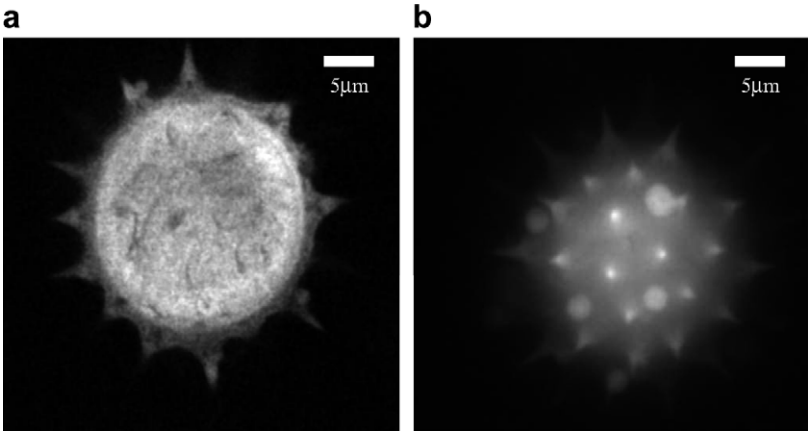

Fig. 9. (a) A typical two photon fluorescence image of a pollen grain exhibiting sectioning. (b) A typical extended depth of focus two photon fluorescence image of a pollen grain taken in a single scan. Line averaging was used to improve the SNR whereby each line in the image was measured four times and averaged to produce the final result.

Finally, we demonstrate a further application of our extended depth of focus PSF to high resolution two photon stereoscopic microscopy. In a conventional stereo microscope each eye views the object through a slightly different angle [19]. This results in a lateral separation of the left- and right-hand images of each object point, the magnitude of which depends on the axial distance from the focal plane. In this way the observer gains a sense of depth perception in an image.

It is clear from Fig. 9b that images taken with our system appear to be viewed along one particular direction. This direction is in fact defined by the orientation of the PSF and by changing this orientation we can change the effective viewpoint. Fig. 10 shows how we can change the PSF orientation by introducing a lateral shift to the annular illumination. An example is shown in Fig. 11 where two images taken with the PSF oriented at $\pm 6°$ to produce a high resolution stereoscopic image pair are shown. The lateral shift, Δ, of the annulus may be written in terms of the parallax angle, δ, from geometric considerations as

$$\Delta x = \delta f_0 \cos\gamma \tag{15}$$

where γ is the angle of convergence to the focal point when the ring illumination is centred on the objective lens pupil.

We would like to emphasize that the extended depth of focus imaging and the ability to produce high resolution stereo images are intrinsically linked to each other. Stereo imaging relies on the parallax effect, i.e. apparent lateral shift of the parts of the object that are outside the focal plane when the point of view is changed. Unless one has access to extended depth of focus imaging those out of focus features would be either blurred (as in conventional microscopy) or not visible at all (in the case of confocal or two photon microscopy). Extended depth of focus is therefore a necessary prerequisite for high-resolution parallax based stereo microscopy.

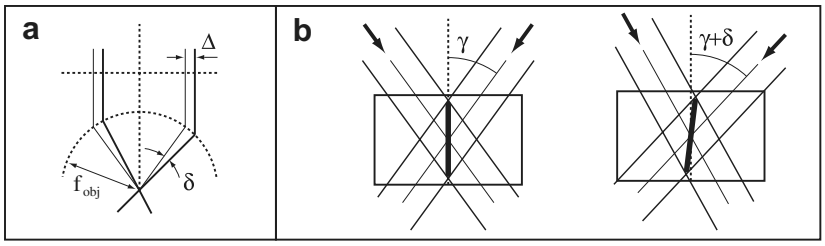

Fig. 10. Laterally shifting the annular pupil function results in a change of parallax angle for the extended PSF. This is shown geometrically in (a) and a closeup of the focal region is shown in (b).

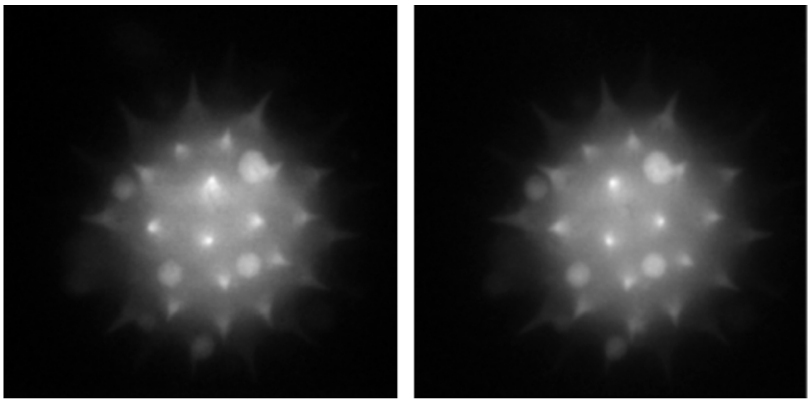

Fig. 11. A stereoscopic image pair taken with an extended depth of focus PSF in two photon fluorescence mode. Line averaging was used to improve the SNR in each.

4. Conclusion

In this paper we have described the use of a binary phase-only grating to produce a ring-shaped distribution of light as an intermediate step in the production of high NA Bessel beams for scanning microscopy. We have shown that this simple and relatively inexpensive diffractive element was able to produce the required beam with efficiency exceeding 75%. This enabled us for the first time to obtain two photon fluorescence images with a depth of field extended by more than an order of magnitude. Moreover, we introduced a further step of spatial filtering in the Fourier plane of the mask which enabled us to fine tune the axial profile of the illumination PSF and thus achieve a near constant image intensity throughout the depth of field. It has to be emphasized that all these enhancements in depth of field were achieved without compromising the lateral resolution of the microscope. The potential scope of application of this method was further broadened by demonstrating a stereo imaging capability. This was achieved by obtaining a pair of extended depth of field images from different viewing parallaxes by employing tilted PSFs.

Acknowledgements

This work was supported by the Basic Technology grant from Research Councils UK, the Department of Health and Carl Zeiss GmbH. We would like to acknowledge contributions to this work by Mark Neil, Farnaz Massoumian and Richard Cook.

References

[1] G. Toraldo di Francia, Nuovo Cimenta Suppl 9 (1952) 426.
[2] Z. Zalevsky, D. Mendlovic, Optical Superresolution, Springer, 2004.
[3] M.A.A. Neil, R. Juškaitis, T. Wilson, Z.J. Laczik, V. Sarafis, Opt. Lett. 25 (2000) 245.
[4] C. Ibanez–Lopez, G. Saavedra, G. Boyer, M. Martinez–Corral, Opt. Express 13 (2005) 6168.
[5] M.J. Booth, M.A.A. Neil, R. Juškaitis, T. Wilson, Proc. Natl. Acad. Sci. USA 99 (2002) 5788.
[6] S. Quabis, R. Dorn, M. Eberler, O. Glockl, G. Leuchs, Opt. Commun. 179 (2000) 1.
[7] M.A.A. Neil, F. Massoumian, R. Juškaitis, T. Wilson, Opt. Lett. 27 (2002) 1929.
[8] T. Wilson, in: H. Masuhara, S. Kawata (Eds.), Nanophotonics, Elsevier, 2004.
[9] L.M. Soroko, Meso-Optics, World Scientific, 1996.
[10] W.T. Welford, J. Opt. Soc. Am. 50 (1960) 749.
[11] C.J.R. Sheppard, T. Wilson, Appl. Opt. 18 (1979) 3764.
[12] Max Born, Emil Wolf, Principles of Optics, sixth ed., Pergamon Press, 1983.
[13] L.M. Soroko, in: E. Wolf (Ed.), Progress in Optics, vol.28, North-Holland, 1989.
[14] W.J. Denk, J.P. Strickler, W.W. Webb, Science 248 (1990) 73.
[15] J.W. Goodman, Introduction to Fourier Optics, second ed., McGraw-Hill, 1996.
[16] E. Wolf, B. Richards, Proc. Roy. Soc. A 253 (1959).
[17] T. Wilson, R. Juškaitis, P. Higdon, Opt. Commun. 141 (1997).
[18] T. Wilson, C.J.R. Sheppard, Theory and Practice of Scanning Optical Microscopy, Academic Press, London, 1984.
[19] D. Birchon, Optical Microscopy Technique, Newnes, London, 1961.